



Research paper

Slow motility in hair cells of the frog amphibian papilla: Myosin light chain-mediated shape change

Nasser A. Farahbakhsh^{a,*}, Peter M. Narins^{a,b}

^a Department of Physiological Science, 621 Charles E. Young Drive S., University of California, Los Angeles, CA 90095-1606, USA

^b Department of Ecology and Evolutionary Biology, 621 Charles E. Young Drive S., University of California, Los Angeles, CA 90095-1606, USA

ARTICLE INFO

Article history:

Received 2 October 2007

Received in revised form 10 April 2008

Accepted 14 April 2008

Available online 29 April 2008

Keywords:

Auditory hair cells

Kinase/phosphatase dependence

Iso-volumetric shortening

ABSTRACT

Using video, fluorescence and confocal microscopy, quantitative analysis and modeling, we investigated intracellular processes mediating the calcium/calmodulin ($\text{Ca}^{2+}/\text{CaM}$)-dependent slow motility in hair cells dissociated from the rostral region of amphibian papilla, one of the two auditory organs in frogs. The time course of shape changes in these hair cells during the period of pretreatment with several specific inhibitors, as well as their response to the calcium ionophore, ionomycin, were recorded and compared. These cells respond to ionomycin with a tri-phasic shape change: an initial phase of iso-volumetric length decrease; a period of concurrent shortening and swelling; and the final phase of increase in both length and volume. We found that both the myosin light chain kinase inhibitor, ML-7, and antagonists of the multifunctional $\text{Ca}^{2+}/\text{CaM}$ -dependent kinases, KN-62 and KN-93, inhibit the iso-volumetric shortening phase of the response to ionomycin. The type 1 protein phosphatase inhibitors, calyculin A and okadaic acid induce minor shortening on their own, but do not significantly alter phase 1 response. However, they appear to counter effects of the inhibitors of $\text{Ca}^{2+}/\text{CaM}$ -dependent kinases. We hypothesize that an active actomyosin-based process mediates the iso-volumetric shortening in the frog rostral amphibian papillar hair cells.

© 2008 Elsevier B.V. All rights reserved.

1. Introduction

In addition to the prestin-mediated ultra-fast electromotility (Dallos and Fakler, 2002), mammalian outer hair cells (OHCs) also exhibit a “slow” motility, in the form of length changes with a rather variable time scale, from microseconds to minutes (Schacht et al., 1995; Dallos et al., 1997; Puschner and Schacht, 1997). Slow motility has been suggested to act as a “gain control” mechanism that modulates or adapts the positive feedback provided by the OHCs’ electromotile apparatus (Lim and Kalinec, 1998), and provides some protection against acoustic overstimulation (Reiter and Liberman, 1995). Slow motility in OHCs can be induced by a number of biochemical agents, including the presumed efferent nerve neurotransmitter, acetylcholine (ACh). ACh binds to and activates the ionotropic nicotinic cholinergic receptor in the OHCs, and induces an inward cationic current predominantly carried by

Ca^{2+} (Blanchet et al., 1996). Strategically-located Ca^{2+} -activated K^{+} channels translate the Ca^{2+} entry into K^{+} exit, leading to the cell membrane hyperpolarization, in the micro- to milli-second time scale (Housley et al., 1992), changing the operating point of the prestin motor.

The signal transduction cascades mediating the slower components of the ACh effect on OHCs are not completely understood. ACh promotes a reduction in the OHCs’ global stiffness, and thus an increase in the magnitude of electromotility (Dallos et al., 1997), possibly by causing Ca^{2+} -dependent phosphorylation of some elements of the OHCs’ cortical lattice (Szonyi et al., 1999a). However, OHCs’ stiffness has also been found to be voltage-dependent (He and Dallos, 1999). More recent studies suggest that up to 54% of the global stiffness is contributed by the prestin-containing plasma membrane, which is also modulated by ACh (He et al., 2003a). Frolenkov et al. (2000) suggested that intracellular calcium ($[\text{Ca}^{2+}]_i$) both modulates the OHCs’ cytoskeletal stiffness, and shifts the voltage sensitivity of the electromotile mechanism. The effects of the $[\text{Ca}^{2+}]_i$ increase on electromotility could be inhibited by the calmodulin antagonists, W-7 (Szonyi et al., 2001) and trifluoperazine, as well as by KN-62, an inhibitor of the multifunctional $\text{Ca}^{2+}/\text{calmodulin}$ -dependent kinases (Sziklai et al., 2001). In addition, Ca^{2+} -independent regulatory mechanisms involving cGMP- (Szonyi et al., 1999) and Rho-GTPases (Kalinec et al., 2000; Zhang

Abbreviations: AP, amphibian papilla; $[\text{Ca}^{2+}]_i$, intracellular free calcium concentration; CaM, calmodulin; CaMK, multifunctional $\text{Ca}^{2+}/\text{CaM}$ -dependent kinase; DIC, differential interference contrast; DMPP, 1,1-dimethyl-4-henylpiperazine iodide; MLC, myosin light chain; MLCK, myosin light chain kinase; MLCP, myosin light chain phosphatase; OHC, outer hair cells; RAPHC, rostral AP hair cell

* Corresponding author. Tel.: +1 310 206 4343.

E-mail address: farahbak@ucla.edu (N.A. Farahbakhsh).

et al., 2003) dependent phosphorylation/dephosphorylation of different elements of the electromotile machinery have been proposed. While the cGMP-dependent pathway may target the prestin motor itself (Deak et al., 2005), the Rho-GTPase-activated cascade is suggested not to affect the prestin function (Zhang et al., 2003). A notable difficulty in the study of slow motility in OHCs has been the inability to isolate and investigate separately the contribution of either cytoskeleton or the electromotile protein. He et al. (2003a) were able to abolish prestin activity in OHCs by replacing the intracellular Cl^- with pentane sulfonate. These experiments may offer a way to study the role of non-prestin elements in the OHCs' slow motility, in isolation. However, it needs to be shown that intracellular Cl^- replacement would not significantly affect the activity of non-prestin components mediating slow motility.

While hair cells in non-mammalian vertebrates share many essential characteristics with their mammalian counterparts, they appear to lack an electromotile protein in their plasma membrane (He et al., 2003; Köppl et al., 2004). As such, auditory hair cells in non-mammalian vertebrates provide us with a simple model to study the contribution to slow motility of intracellular pathways modulating the cytoskeletal structure, and thus hair cells' geometrical shape, without the influence of voltage-dependent transmembrane motile elements. Our goal is to provide a basis for comparing the process of auditory hair cell slow motility in an amphibian with that of its mammalian counterpart. Our research on the auditory hair cells of the amphibian papilla, one of the two auditory organs in the frog, has demonstrated that long rostral hair cells in this organ, which are the predominant recipients of the efferent innervation (Simmons et al., 1995), but not shorter hair cells from the medial and caudal regions of this organ, modulate their length in response to application of neurotransmitters, acetylcholine and ATP, as well as the calcium ionophore, ionomycin (Farahbakhsh and Narins, 2004). The effects of acetylcholine could be mimicked by carbachol and DMPP. However, the effect of the latter agonist appeared to be irreversible (Farahbakhsh and Narins, unpublished observations).

In a recent report (Farahbakhsh and Narins, 2006) we provided evidence suggesting that in the rostral AP hair cells (RAPHCs) of the northern leopard frog, *Rana pipiens pipiens*, increases in the $[\text{Ca}^{2+}]_i$ promote cell shape change. These changes are composed of two partially-overlapping shortening phases: an initial rapid iso-volumetric contraction (phase 1), and a slower length decrease accompanied with swelling (phase 2), suggesting movement of salt and water across the cell membrane in the latter phase. Usually, shortening was followed by a period of slow increase in both length and volume (phase 3). We showed that it was possible to unmask the iso-volumetric contraction by delaying the cell swelling with the help of the K^+ or Cl^- channel inhibitors, quinine or furosemide. Furthermore, we demonstrated that the initial longitudinal contraction (phase 1) in these cells is Ca^{2+} /calmodulin (Ca^{2+} /CaM)-dependent: in the presence of W-7 only a slow phase 2 response could be observed. These findings suggested that similar to the mammalian auditory outer hair cells, the amphibian rostral AP hair cells possess a Ca^{2+} /CaM-dependent contractile mechanism capable of mediating length changes in response to extracellular stimuli.

In the present work, we have identified those processes controlled by Ca^{2+} and calmodulin that might participate in the iso-volumetric shortening response of RAPHCs to ionomycin. We investigated the effects of three inhibitors of Ca^{2+} /CaM-dependent kinases, and two inhibitors of type 1 protein phosphatase. Our results suggest that phosphorylation/dephosphorylation of myosin light chain (MLC) may regulate the speed and extent of length decrease during phase 1 response (see Fig. 7). We hypothesize that iso-volumetric shortening in RAPHCs is mediated by an active

actomyosin-based mechanism. Preliminary reports of these findings were presented at the 2006 and 2007 meetings of the Association for Research in Otolaryngology (Farahbakhsh et al., 2006; Farahbakhsh and Narins, 2007).

2. Methods

2.1. Dissociation of hair cells

Amphibian papillae (APs) were dissected out of pithed and decapitated adult northern leopard frogs (*Rana pipiens pipiens*), and hair cells were gently scraped free from trypsin-treated APs in the recording chamber as described recently (Farahbakhsh and Narins, 2006). The recording chamber was then placed on the stage of an inverted microscope (Zeiss IM, Germany), and the hair cells were continuously perfused with the AP solution, a perilymph-like standard external solution (Bernard et al., 1986). The AP solution contained (in mM): NaCl, 110; KCl, 2; CaCl_2 , 2; MgCl_2 , 0.8; D-glucose, 3; HEPES, 10. pH was adjusted to 7.2, with NaOH. Osmolarity was adjusted to 223–227 mosmol l^{-1} with a vapor pressure osmometer (Vescor, model 5520, Logan, UT).

2.2. The chamber and experimental setup

The recording chamber consisted of a 35 mm plastic petri dish, specially modified by cutting a hole about 14 mm in diameter into its bottom and cementing a 25-mm microscope glass cover slip under the hole with paraffin. A plastic insert was placed in the petri dish to reduce the effective volume of the chamber to 300 μl , to provide an input and output for the perfusion system and to hold the thermometer probe. The rate of perfusion of cells was 1.4–2 ml/min, which was maintained throughout each experiment. In order to record the complete time course of the shape change, we started each experiment by perfusing the hair cells for 10–15 min with the AP solution, then treated them with inhibitors and ionomycin through continued perfusion for durations exceeding 10 min, and finally, washed out these chemicals by perfusing with the AP solution alone. We ended every experiment by exposing the cell to a hypo-osmotic solution. The experimental data was accepted only if the cell responded to the hypo-osmotic shock with further swelling, and intracellular granulation, indicating that the cell membrane had remained intact throughout the experiment.

The microscope was equipped with a 100x/1.3 oil-immersion plan-neofluar objective (Zeiss) and components of the differential interference contrast (DIC) microscopy. A CCD camera (model CCD-72, Dage-MTI, Michigan City, IN) were used to collect the DIC images which were then displayed on a video monitor, acquired by the image acquisition board for on-line analysis, and recorded on videotape.

2.2.1. Hair cell length and volume measurements

For the off-line data analysis, individual DIC images were digitized and displayed on the computer screen, and the contour of the hair cell soma was traced manually. Then, the contour line was analyzed using custom-made software to determine the cell's length and cross-sectional area. The cell's average diameter and volume were estimated as described previously (Farahbakhsh and Narins, 2006). Since the images are acquired at video rate, it is possible to follow the time course of changes in these four parameters at the rate of 30 measurements per second. However, for the experiments reported in this manuscript, it appeared that analyzing one image per minute would be sufficient for most of the experiments, except during the period of rapid shape change in response to ionomycin (e.g. in Figs. 2 and 3) for which up to six images per minute were analyzed.

2.2.2. Data analysis

Changes in the measured length and estimated somatic volume were calculated and compared between different episodes in each experiment, and between similar experiments. In addition we determined the iso-volumetric fraction of total shortening ($\delta L_{\text{iso-v}}/\delta L_{\text{Total}}$) for the duration of exposure to ionomycin. For the sake of brevity, however, the parameters presented and discussed are limited to only those required to show a significant drug-induced effect. The assembled data for each group of similar experiments was summarized and presented as mean \pm standard deviation (Fig. 6). Statistical significance was determined using the one-way ANOVA, as indicated. $p < 0.05$ was considered statistically significant.

2.2.3. Model

For the analysis of shape changes in rostral amphibian papillar hair cells, we modeled the cell's soma as a truncated prolate spheroid that provided a better approximation than the cylindrical model used for the outer hair cells (Iwasa and Chadwick, 1992). Details of the development and application of this model to RAPHCs are previously reported (Farahbakhsh and Narins, 2006). Briefly, the model assumes that the three-dimensional geometry of the hair cell can be approximated by a stack of thin slices cut perpendicular to the longitudinal axis of the cell. Each slice is composed of two semi-circular cylinders whose radius is equal to the distance between hair cell's axis and contour in that slice. The thickness of each slice is no more than one image pixel (0.16 μm). Thus, the volume of the hair cell is predicted to be the same as the sum of the volumes of all such thin semi-circular cylinder pairs.

In order to validate this model, we utilized a laser scanning confocal microscope (Leica, model TCS SP). Cells were loaded with the Ca^{2+} -sensitive fluorescent dye, Fluo-3 (Molecular Probes, Eugene, OR), and excited with the 488-nm line of an argon laser beam. The emitted light between 500 and 550 nm was collected. The hair cell was placed diagonally in a 40 μm by 40 μm square area, which was scanned by the laser beam to form a 512- by 512-pixel confocal image (resolution, 0.078 μm per pixel). In order to construct a three-dimensional image of the cell, the scanning plane was moved along the z-axis in steps of either 0.1 or 0.5 μm . A video clip showing the 3D image of a RAPHC is posted at <http://www.physci.ucla.edu/farahbakhsh/HAIR/3D.html>. Fig. 1A and B shows selected horizontal and vertical profiles of this cell's 3D reconstruction, before and after application of 5 μM ionomycin, respectively. As is demonstrated in these profiles, the confocally imaged hair cell appears to have a depth larger than what its width suggests. As shown in Fig. S1 of the Supplementary material, such an anomaly is a direct result of light scattering in optical systems (e.g., the confocal microscope), that leads to spreading (blurring) of images, and thus the egg-shape appearance of spherical objects. Fig. 1C and D shows the result of deconvolution of images in Fig. 1A and B, respectively. For deconvolution, we used both a theoretical point spread function (PSF) included in the deconvolution software (AxioVision, Zeiss, Germany), as well as the PSF we measured with our confocal microscope, by imaging a 0.1- μm fluorescent bead (Tetra-speck Microsphere, Invitrogen, Carlsbad, CA). Whereas, depending on the strength of deconvolution used (mild, moderate or strong), either PSF could remove a significant part of the halo surrounding the image of hair cells, neither was able to completely correct the distortion in vertical profiles (see Figs. 1C and D, and S1).

Despite artifactual deformation of the confocal images it was still possible to validate our model. Fig. S2 shows the relationship between the volumes predicted by our model with those measured with confocal microscopy for five RAPHCs, after deconvolution (using a moderate strength). The volume of each cell is shown before (solid symbols) and after (open symbols) treatment with 5 μM ionomycin. The slope of the regression line is 1.19, and the corre-

lation coefficient >0.99 . The ratio of volumes measured by the confocal microscope and predicted by our model was very close to 1.19 for four RAPHCs. This figure is also very close to the ratio of the profiles for the 4.2 μm -diameter spherical bead shown in Fig. S1: 1.21, for the moderate deconvolution with either PSF; 1.18 and 1.14, for the strong deconvolution with theoretical and measured PSFs, respectively. If we calibrate our measurements with the confocal microscope, using the ratio of 1.19, we find that our model can predict the RAPHCs' volume with an accuracy of about 2%, despite the large changes in cells' shape observed as a result of treatment with ionomycin.

It should be mentioned that for the fifth cell (the smallest in Fig. S2), the volume ratio was 1:31. We attribute this deviation to the fact that this cell did not adhere to the underlying glass coverslip, and its longitudinal axis was quite tilted with respect to the image plane. As a result, this cell's volume was underestimated by our model. The data from similar tilted cells are not included in this study.

2.2.4. Measurement of intracellular Ca^{2+} concentration

For $[\text{Ca}^{2+}]_i$ measurements, fura 2/AM (Molecular Probes, Eugene, OR) was dissolved in DMSO at a final concentration of 5 μM (DMSO would be diluted 1000 times). The hair cells placed in the recording chamber were loaded with fura 2 in the AP solution for up to 30 min. This was followed by a 15–30 min washout and equilibration period which we have found necessary for stable $[\text{Ca}^{2+}]_i$ measurements. The excitation wavelengths were 340 and 380 nm, and fluorescence emission was collected with an 80-nm-wide band-pass filter centered at 510 nm (Tsien et al., 1985). During each experiment, fluorescence intensity of several regions of interest (ROI) along the length of the cell or just outside its boundary were recorded, and the fluorescence level for all pixels within each ROI was separately averaged for each excitation wavelength, and their time-courses were followed (see Fig. 3A and C). In addition, the fluorescence intensity in an area of the image devoid of any cell or debris was recorded for each excitation wavelength, and used as the background intensity to be subtracted from the fluorescence intensity of each ROI. The fluorescence-ratio (R), was calculated for each ROI as,

$$R = S'_{340}/S'_{380} = (S_{340} - S_{\text{BG},340})/(S_{380} - S_{\text{BG},380}),$$

where S_{340} and S_{380} are the average fluorescence intensity emitted in each ROI as a result of excitation at 340 and 380 nm, respectively; $S_{\text{BG},340}$ and $S_{\text{BG},380}$, the background intensities; S'_{340} and S'_{380} are the background-subtracted intensities for each ROI.

We estimated the $[\text{Ca}^{2+}]_i$ at each time point in accord with the method of Grynkiewicz et al. (1985):

$$[\text{Ca}^{2+}]_i = \beta \times K_d \times (R - R_{\text{min}})/(R_{\text{max}} - R),$$

where K_d is fura-2's dissociation constant for Ca^{2+} ; R_{min} and R_{max} are the fluorescence-ratio in zero and saturating concentrations of calcium, respectively. β is the ratio of fluorescence intensities in zero and saturating $[\text{Ca}^{2+}]_i$ when fura-2 is excited at 380 nm ($\beta = S'_{f380}/S'_{b380}$, where subscripts f and b stand for the Ca^{2+} -free and bound forms of fura-2).

A large increase in the cell volume during phases 2 and 3 of response to ionomycin significantly lowers the intracellular medium's ionic strength (which affects dye's dissociation constant for Ca^{2+}), and dilutes fura-2 (that decreases the fluorescence intensity and thus the signal-to-noise ratio). Because of these technical difficulties, we did not calibrate the absolute values of the $[\text{Ca}^{2+}]_i$ in every experiment. However, in six experiments we were able to limit the ionomycin-induced hair cells' volume change by increasing the osmolarity of the calibration media with addition of 100 mM sucrose. Lower concentrations of sucrose were not as

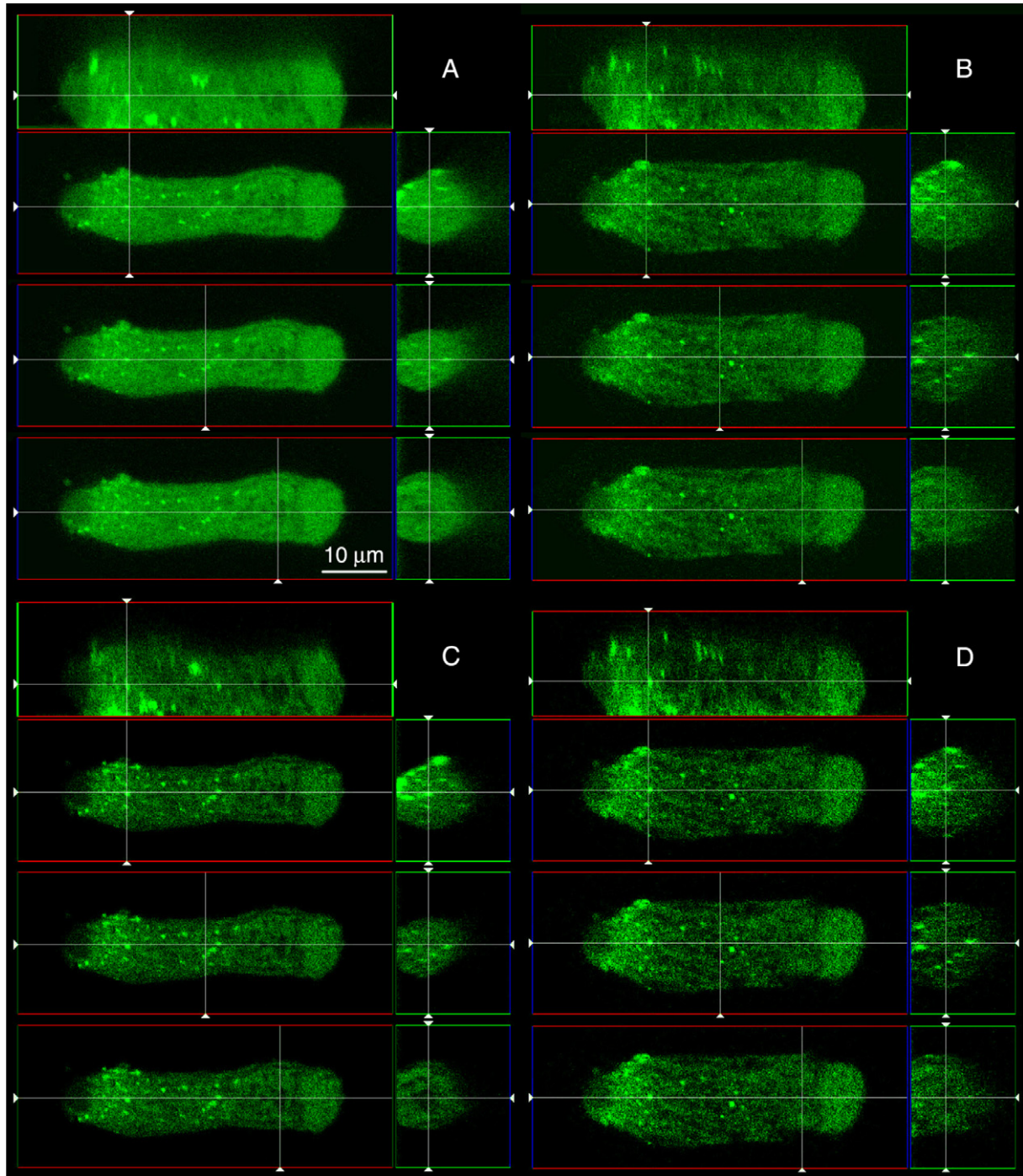


Fig. 1. Confocal microscopy of a RAPHC: (A) Selected profiles of the RAPHC before treatment with ionomycin. The vertical-axial (top panel), horizontal (three lower left panels), and three transverse (right panels) profiles of a 3D-reconstructed image of the RAPHC are shown. The position of the transverse profiles are indicated by vertical lines in their respective left panels (horizontal cross section). (B) Similar profiles of the RAPHC after it was treated with 5 μM ionomycin. (C) The same 3D image as in A, after deconvolution with the measured PSF, with moderate-strength. (D) The same 3D image as in B, after moderate-strength deconvolution with the measured PSF.

effective. Our calibration media had the following compositions: for measuring R_{max} and S'_{b380} , (in mM): KCL, 113; CaCl_2 , 2; MgCl_2 , 0.8; D-glucose, 3; HEPES, 10. To maximize the rate of calcium exchange across the cell membrane, 10 μM ionomycin and 100 μM carbonyl cyanide 3-chlorophenylhydrazine (CCCP) was added to this medium. For measuring R_{min} and S'_{f380} , CaCl_2 was removed from the above solution, and 3 mM KCl and 1 mM EGTA were added. Osmolarity and pH of both solutions were adjusted to 320 mOsm and 7.2, respectively.

Furthermore, in order to correct for the small volume changes in these RAPHCs between the times S'_{b380} and S'_{f380} were measured, we modified β as,

$$\beta = (S'_{f380}/S'_{b380}) \times (V_{f380}/V_{b380}),$$

in which V_{f380} and V_{b380} are the cell volume at the time of measuring S'_{f380} and S'_{b380} , respectively. In the six experiments we conducted in hyper-osmotic calibration media, this correction factor was 1.08 ± 0.16 (range, 0.87–1.27). The average values for R_{min} , R_{max}

and corrected β were 0.22, 2.54 and 4.08, respectively. A K_d of 224 nM was used (Grynkiewicz et al., 1985).

2.2.5. Chemicals

W-7, ML-7, KN-62 and KN-93 were purchased from Biomol (Plymouth Meeting, PA). Ionomycin was obtained from Molecular Probes (Eugene, OR). Other chemicals were purchased from Sigma. Ionomycin, CCCP and all inhibitors were dissolved in DMSO, and the stock solutions were kept at -20°C . At the time of experiment, ionomycin or inhibitors stocks were diluted into the AP solution. The final concentration of DMSO in the AP solution was kept at 0.1%, or less.

2.2.6. Animal care

The care and use of animals reported in this study were approved by the University of California at Los Angeles Chancellor's Animal Research Committee (ARC number 1994-086-41).

3. Results

Auditory hair cells dissociated from the rostral region of the frog's amphibian papilla (RAPHCs) maintain their geometrical shape for a period exceeding one hour while continuously perfused with a perilymph-like solution (AP solution; for composition, see Methods). We have recently reported (Farahbakhsh and Narins, 2006) that it is possible to induce shape change in RAPHCs by varying their intracellular calcium concentration ($[\text{Ca}^{2+}]_i$). For example, raising the $[\text{Ca}^{2+}]_i$ by exposing these cells to the calcium ionophore, ionomycin, would lead to a three-part shape change. During the first two parts (to which we referred as phases 1 and 2), RAPHCs shorten, while during the last part of the response to ionomycin (phase 3) they lengthen. In phase 1, the cell contracts longitudinally while maintaining its volume (iso-volumetric shortening). During phase 2, however, further shortening is accompanied by volume increase ("osmotic" response). Fig. 2 shows DIC and fluorescence-ratio images spanning a 6-min period during exposure of a $51\text{-}\mu\text{m}$ RAPHC to $5\text{ }\mu\text{M}$ ionomycin. The images in the top panels were acquired at the start of perfusion with the ionophore. Fifteen seconds later, the $[\text{Ca}^{2+}]_i$ started to rise (see Fig. 3A), while the cell's shape remained unchanged for the first two minutes. The panels in second row of Fig. 2 show DIC and fluorescence-ratio images of the cell 135 s after the start of perfusion with ionomycin. The pseudo-colored ratio image shows a considerable increase in the $[\text{Ca}^{2+}]_i$, while the change in the cell's length, in the DIC image, is negligible. As shown in the three middle-row panels, within the following 43 s, the cell shortened by $9.5\text{ }\mu\text{m}$ (19%), while the $[\text{Ca}^{2+}]_i$ rise continued. In the next 40 s, the cell's length rebounded by $1.5\text{ }\mu\text{m}$ (3%). Throughout this 83-s period of length and $[\text{Ca}^{2+}]_i$ changes, the cell's volume remained unchanged. The bottom two rows of panels in Fig. 1 shows the period referred to as 'osmotic' shortening (phase 2).

Fig. 3A shows the complete time-course of changes in this RAPHC's length, volume and $[\text{Ca}^{2+}]_i$ (in four selected regions), during the period of exposure to ionomycin. As shown in Fig. 3C, these four regions were selected such that in addition to following the local changes in the $[\text{Ca}^{2+}]_i$, variations in the cell's length and diameter also could be displayed. Regions 1 and 5 are positioned near the two ends of the RAPHC, whereas regions 6 and 7 are along the sides of the cell. As such, regions 1 and 5 show a parallel decrease in the $[\text{Ca}^{2+}]_i$ when the cell shortens, and regions 6 and 7 display a $[\text{Ca}^{2+}]_i$ rise as the cell's diameter increases. These parallel changes can be seen in Fig. 3A. In the first 135 s after the start of ionomycin perfusion, the $[\text{Ca}^{2+}]_i$ in regions 1 and 5 (green and cyan traces) increases, while the length (black squares), volume (grey squares) and calcium level in regions 6 and 7 (blue and magenta

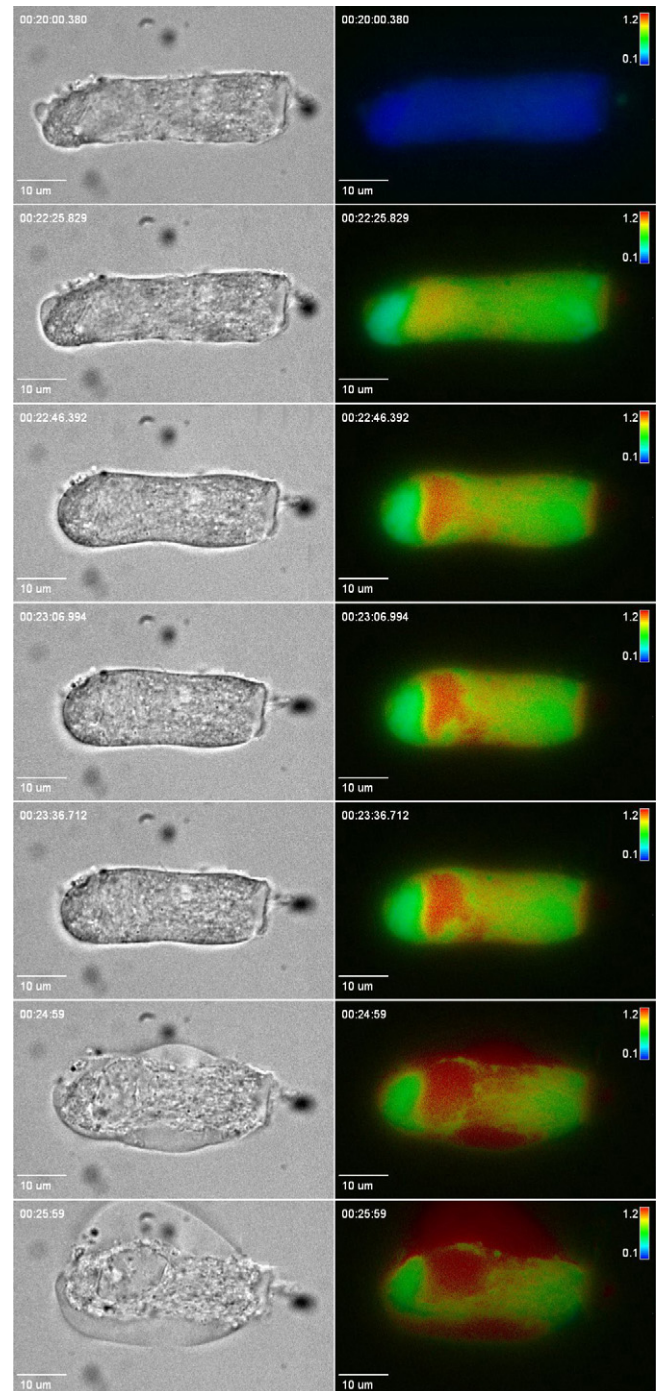


Fig. 2. Ionomycin-induced shape change of a RAPHC. Time-lapse photography of a RAPHC's shape and intracellular calcium changes during exposure to $5\text{ }\mu\text{M}$ ionomycin. The elapsed time between the start of the experiment and the time the DIC and fluorescence-ratio image pairs were recorded is shown (in hr:min:s) in each panel. The horizontal scale bar represents $10\text{ }\mu\text{m}$. The fluorescence-ratio images were pseudo-colored according to the color scale bar shown on the right.

dashed lines) show no change. In the next 43 s, the length and $[\text{Ca}^{2+}]_i$ in regions 1 and 5 drop, the calcium levels in regions 6 and 7 increase, but the volume still remains unchanged. During the length rebound in the next 40 s, $[\text{Ca}^{2+}]_i$ in the four selected regions follow the shape change accordingly. Finally, the volume increase (starting 4 min into the ionomycin treatment) is accompanied by both shortening and dilution of the fluorescent dye as indicated by the drop in fluorescence signals in all four regions.

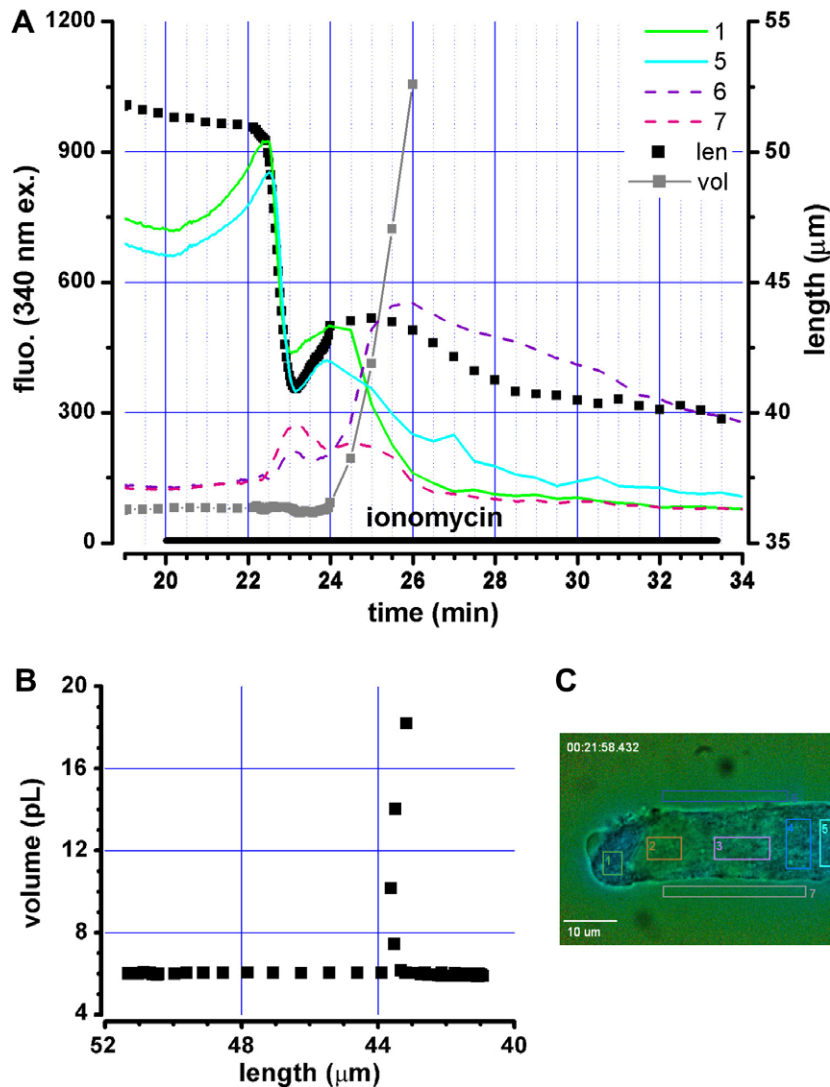


Fig. 3. Quantification of shape change: (A) Time-courses of changes in the length (black squares), volume (grey squares), and fluorescence signal (340 nm excitation) for the cell in Fig. 2. Changes in the RAPHC's length (in μm) and estimated volume (arbitrary units), and fluorescence signal in four regions of interest (ROIs, marked in C), during exposure to the calcium ionophore are shown. The bar below shows the duration of treatment with ionomycin. (B) The length–volume relationship for this cell during treatment with ionomycin shows a sizable iso-volumetric length change, followed by swelling. Volume is given in picoliter ($=10^3 \mu\text{m}^3$), length in μm . (C) Positions of ROIs used for the display of fluorescence time course in A are marked. Notice that before the start of shape change (time, 21:58.432), ROIs 1 and 5 were on the cell's soma, near the ends, whereas ROIs 6 and 7 were positioned along the cell, just outside its border.

Subsequent calibration of the free calcium level in this cell (see Methods for details) suggests that $[\text{Ca}^{2+}]_i$ was 79 nM before the application of ionomycin, rose to 1.3 μM when shortening was first detected, and reached 3.8 μM when shortening was at its highest rate. In seven similarly calibrated experiments, the corresponding $[\text{Ca}^{2+}]_i$ levels were 66 ± 19 nM, 1.2 ± 0.7 μM and 3.6 ± 1.6 μM , respectively. It should be added that ionomycin, as a $\text{Ca}^{2+}/\text{H}^+$ exchanger (Erdahl et al., 1994), causes intracellular alkalization in cells bathed in solutions with physiological level of Ca^{2+} . Our own measurements suggest that in RAPHCs, 5 μM ionomycin can induce up to 0.5 pH unit of intracellular alkalization (Farahbakhsh et al., 2006). The effects of this alkalization on the shape change, however, are not clear; Alkalizing RAPHCs up to 1 pH unit, with 25 mM NH_4Cl , failed to produce a significant iso-volumetric shortening (data not shown).

The length–volume relationship shown in Fig. 3B clearly demonstrates the distinct iso-volumetric length change at the start of this RAPHC's ionomycin-induced shape change. For the RAPHC shown in Figs. 2 and 3, the iso-volumetric length shortening con-

stituted 92% of the total ionomycin-induced length decrease. However, in 10 cells treated with 5 μM ionomycin the iso-volumetric shortening fraction ($\delta L_{\text{iso-v}}/\delta L_{\text{total}}$) was $59 \pm 23\%$ (Fig. 6).

Our previous work (Farahbakhsh and Narins, 2006) has suggested that phase 1 response is calmodulin (CaM) dependent: RAPHCs pretreated with W-7, a CaM inhibitor, exhibited only a purely osmotic (phase 2) response to ionomycin. In what follows, we investigated the possible role of two well-known classes of kinases activated by calmodulin, namely the myosin light chain kinase (MLCK), and multifunctional calcium/calmodulin-dependent kinases (CaMKs).

3.1. Myosin light chain kinase (MLCK)

To examine the possible role of myosin light chain kinase in the ionomycin-induced iso-volumetric shortening, we treated RAPHCs with ML-7, a specific MLCK inhibitor (Saitoh et al., 1987; Bain et al., 2003), for periods exceeding 15 min. At 5 μM concentration, ML-7 applied alone, did not induce a significant change in either length

or volume of RAPHCs (not shown). However, ML-7-pretreated cells responded quite differently to ionomycin than untreated (control) cells. The 51- μm -long cell shown in Fig. 4A was exposed to the combination of 5 μM ML-7 and 5 μM ionomycin following 18 min of pretreatment with the same concentration of ML-7. After a delay of 200 s, an increase in the cell's volume became noticeable (10.7%), while its length was still unchanged. This was found to be a general feature: in contrast with the control cells (Figs. 2 and 3), in ML-7-treated RAPHCs, shortening does not precede swelling ($n = 5$). In the hair cell shown in Fig. 4A, this episode was then followed by a 943-s interval during which the cell shortened by 16.4 μm (32.4%), while its volume increased by another 230% (phase 2). For most of this interval, the length and volume changed almost linearly, as expected from an osmotic response (Dulon et al., 1988). Thus, it appears that the primary effect of ML-7 on RAPHCs is inhibition of the iso-volumetric shortening.

A comparison of these results with the response of W-7-treated RAPHCs to ionomycin (Farahbakhsh and Narins, 2006) indicates that the effects of ML-7 and W-7 on the ionomycin-induced shape change in RAPHCs were quite similar (see Fig. 6).

3.2. Ca^{2+} /CaM-dependent protein kinase(s)

In order to determine whether CaMK activity is present in RAPHCs, we examined the effects of pretreatment with either 5 μM KN-93, or 5.5 μM KN-62, both selective CaMK inhibitors (Tokumitsu et al., 1990; Sumi et al., 1991; Davies et al., 2000). Fig. 4B and C shows the results of two representative experiments ($n = 4$, for each inhibitor). Neither KN-93 nor KN-62, induced a significant shape change in RAPHCs when applied alone (not shown). However, the response of either KN-93- or KN-62-treated cells to ionomycin were qualitatively similar to that of RAPHCs pretreated

with ML-7: the iso-volumetric phase was completely inhibited by both CaMK inhibitors (Fig. 4B and C; see also Fig. 6).

3.3. Are the effects of MLCK and CaMK inhibitors additive?

Since the selective MLCK inhibitor, ML-7 (Saitoh et al., 1987) is a very poor inhibitor of CaMK II (Miralem and Templeton, 1998), and the selective CaMK II and IV inhibitor, KN-62, has a very low affinity for MLCK (Tokumitsu et al., 1990; Davies et al., 2000), our results suggest that both MLCK and CaM kinases II and/or IV, might contribute to the iso-volumetric length change in RAPHCs. Thus, we sought to determine if these two Ca^{2+} /CaM-dependent pathways act in parallel or series. For this purpose, we perfused four RAPHCs with a combination of 5 μM ML-7 and 5.5 μM KN-62, before adding 5 μM ionomycin to the mixture. For the cell in Fig. 4D, the addition of ionomycin to the ML-7 + KN-62 mixture led directly to a phase 2 response (simultaneous shortening and swelling) that started after a delay of 360 s. However, three of the cells in this group exhibited a brief period in which volume increase preceded the length change. In terms of the osmotic response, however similar results were recorded from all four cells (Fig. 6). There was no statistically significant difference between the extent of length or volume change during the osmotic response for the cells in this group and their corresponding parameter for RAPHCs pretreated with ML-7 alone.

3.4. Myosin light chain phosphatase (MLCP)

The data presented so far suggests a role for MLCK in the ionomycin-induced iso-volumetric shortening of RAPHCs. The 20-KD myosin light chain (MLC) is the primary substrate of MLCK (Means, 2000). However, the level of phosphorylation of the MLC is

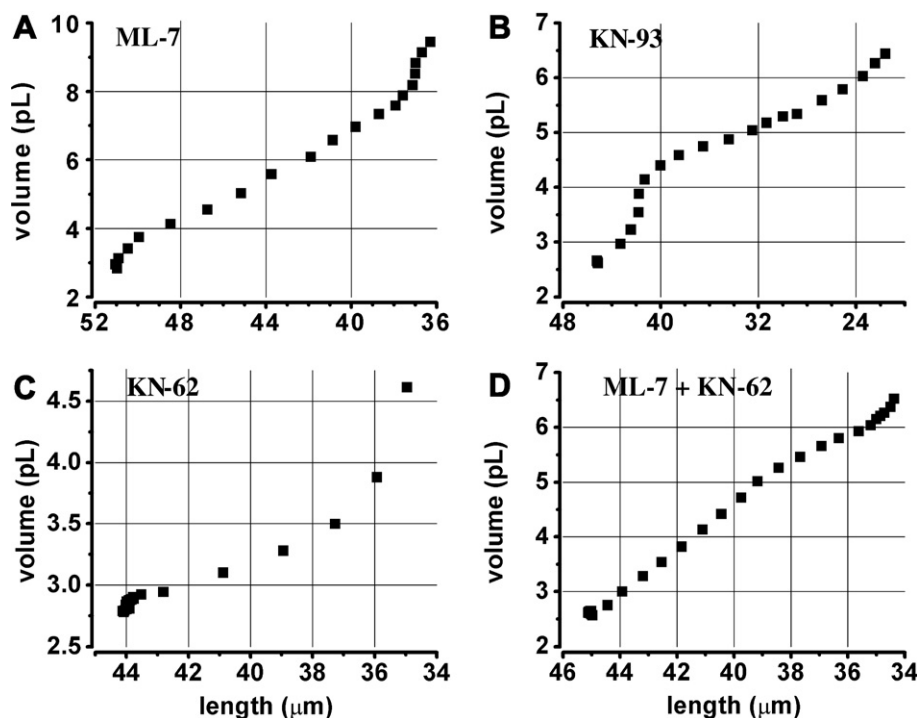


Fig. 4. Effects of several kinase inhibitors on the ionomycin-induced shape change: (A) 15-min pretreatment with the myosin light kinase inhibitor, ML-7, at 5 μM concentration, removes the RAPHC's iso-volumetric shortening. In this cell, the length–volume relationship during treatment with ionomycin showed mainly an osmotic component (parallel changes in the length and volume). (B) and (C) The multifunctional Ca^{2+} /CaM-dependent kinase inhibitors, KN-93 and KN-62 had effects similar to those of ML-7. In RAPHCs pretreated for 15 min with either KN-93 (5 μM , B) or KN-62 (5.5 μM , C), the length–volume relationship during treatment with ionomycin lacked the iso-volumetric shortening episode. (D) Effects of MLCK and CaMK inhibitors are not additive. Ionomycin-induced shape change in a RAPHC pretreated (15 min) with the combination of ML-7 (5 μM) and KN-62 (5.5 μM) was similar to the response of cells pretreated with either inhibitor, alone. The length–volume relationship is that of an osmotic response, with no indication of an iso-volumetric shortening. RAPHCs' length is given in μm , and the estimated volume in picoliters.

determined by the opposing effects of MLCK and MLCP. The catalytic subunit of MLCP is a type 1 phosphatase (PP1) (for a review see Hartshorne et al., 2004). Thus, we tested the effect of two PP1 inhibitors, known to inhibit the smooth muscle myosin phosphatase activity (Ishihara et al., 1989), on the RAPHCs' shape, as well as on the response to ionomycin.

Fig. 5A shows the effect of the PP1 inhibitor, calyculin A. Perfusion with 100 nM calyculin A, for periods of 14–16 min, produced small but statistically significant changes in the cells' length (not shown). Replacing calyculin A with 5 μ M ionomycin led to a three-phase response by RAPHCs. The iso-volumetric character of the initial response to ionomycin is clearly depicted in the length–volume relationship (Fig. 5A). In the five cells treated with calyculin A, 71.7 \pm 29.8% of the total shortening was iso-volumetric (Fig. 6). However, a statistically significant difference with phase 1 response of untreated cells could not be established for calyculin A.

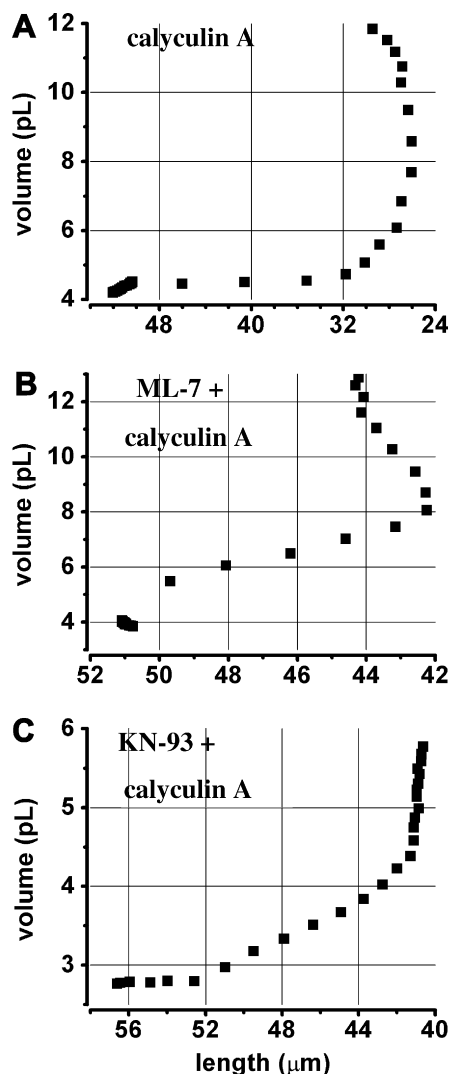


Fig. 5. Effects of the type 1 protein phosphatase inhibitor, calyculin A: (A) Length–volume relationship during exposure to 5 μ M ionomycin in a RAPHC pretreated for 14 min with 100 nM calyculin A shows distinct episodes of iso-volumetric and osmotic shortening. (B) Calyculin A fails to reverse the inhibitory effect of ML-7 on the iso-volumetric shortening. A RAPHC pretreated for 15 min with a combination of 5 μ M ML-7 and 100 nM calyculin A responded to 5 μ M ionomycin with a length–volume relationship without a measurable episode of iso-volumetric shortening. (C) Calyculin A reverses the effect of KN-93. The ionomycin-induced shortening in a RAPHC pretreated for 12 min with 5 μ M KN-93 and 100 nM calyculin A, displayed a significant iso-volumetric component.

The second PP1 inhibitor tested was okadaic acid. Pretreatment with 100 nM okadaic acid, also failed to produce a statistically significant difference in the response to ionomycin ($n = 5$; Fig. 6).

Pretreatment of RAPHCs with a combination of 5 μ M ML-7 and 100 nM calyculin A also failed to reverse the inhibitory effect of ML-7 on the iso-volumetric response to ionomycin (Fig. 5B). In six out of seven similarly pretreated cells the ionomycin-induced shortening lacked a phase 1 component (Fig. 6). Interestingly, however in four out of six RAPHCs pretreated with a combination of 5 μ M KN-93 and 100 nM calyculin A, a significant reversal of the KN-93 inhibitory effect could be observed (Fig. 6). In this group of cells, the iso-volumetric component constituted 20–67% of the total shortening induced by ionomycin. Fig. 5C shows the length–volume relationship during the period of exposure to 5 μ M ionomycin for one of these cells.

4. Discussion

In a recent report (Farahbakhsh and Narins, 2006), we described a calcium-dependent mechanism that can potentially mediate the process of slow motility in low-frequency auditory hair cells of amphibians. Furthermore, we developed a method for quantitative analysis of shape change in isolated hair cells and devised a model for identifying different aspects of the response to agents that modulate the geometrical attributes of these cells. This method allowed us to identify three distinct but temporally overlapping periods in the shape change induced by the calcium ionophore, ionomycin, in hair cells dissociated from the rostral region of the amphibian papilla, one of the two auditory organs in frogs. During phase 1 of the response to ionomycin, these hair cells (RAPHCs) undergo a brief (≈ 50 s long) and slow (≈ 300 nm/s) contraction-like iso-volumetric shortening that in some respects resembles the muscle-like calcium/calmodulin- and metabolism-dependent, gradual and sustained shape change (slow motility) of mammalian outer hair cells (OHCs), first reported in the 1980's (Flock et al., 1986). This episode is then followed by a somewhat longer (≈ 90 s) period during which continued length decrease is accompanied by an increase in the cells' volume (phase 2, or "osmotic" shortening), which has also been observed in OHCs (Dulon et al., 1988). In the last stage of the response (phase 3), the cells' length and volume increase together.

In that work, we relied on a model for estimating the volume of a RAPHC based on a single DIC image of the cell at its largest cross-section. Despite the fact that this model was a refined and improved version of a similar model previously verified and used for the estimation of OHCs' volume (e.g. Chertoff and Brownell, 1994), independent validation of our model was needed. For this purpose, we utilized laser scanning confocal microscopy. Our experiments with this latter system made it clear that because of light scattering and refraction in the optical path, direct and accurate 3D imaging of these cells was not possible (see Section 2 and Supplementary section and figures therein). Nevertheless, using the theoretical and measured point spread functions of the microscope, a 4.2- μ m-diameter fluorescent sphere, and an image deconvolution algorithm, we were able to calibrate our confocal measurements. Comparison of the volume calculated on the basis of calibrated confocal images with that predicted by our model on the basis of the image showing the largest cross-section of the cell (Fig. S2), clearly demonstrates the validity of our model as long as it was applied to RAPHCs whose longitudinal axis was parallel to the image plane (see Supplementary section).

In the present work, we have concentrated our attention on the pathways that may underlie phase 1 response. We have previously reported that this phase is calcium/calmodulin-dependent: removal of calcium from the extracellular medium significantly

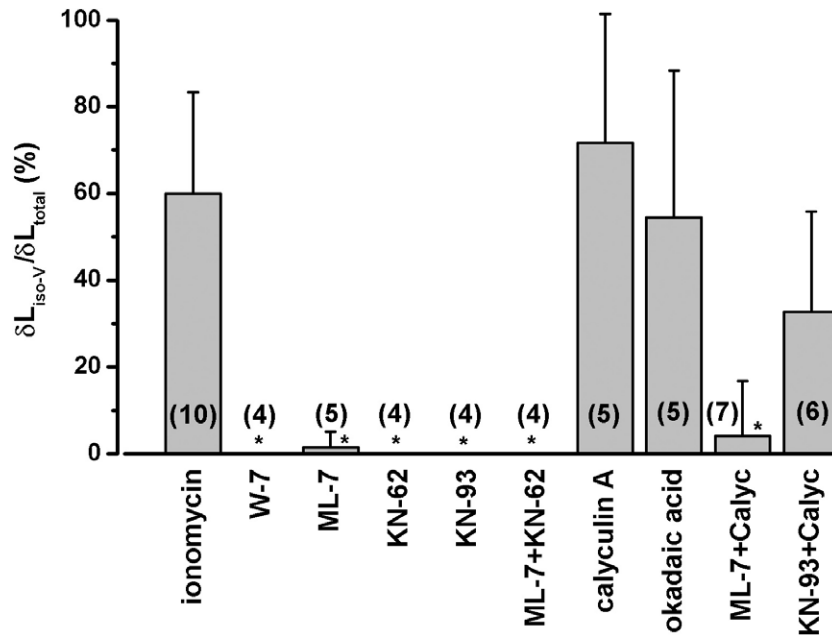


Fig. 6. Data summary. The iso-volumetric fraction of the total length decrease ($\delta L_{iso-v}/\delta L_{total}$) for ten groups of experiments. The data for W-7 is from Farahbakhsh and Narins (2006). The number of RAPHCs in each group is given in parentheses. In cells treated with W-7, KN-62, KN-93 and ML-7 + KN-62, phase 1 episode was completely inhibited. Only one out of six RAPHCs treated with ML-7 had a small iso-volumetric shortening (2.5% of the initial length; $\delta L_{iso-v}/\delta L_{total} = 7.8\%$). Only one out of seven RAPHCs treated with ML-7 + calyculin A had an iso-volumetric response ($\delta L_{iso-v}/\delta L_{total} = 28\%$). (*) represents an average $\delta L_{iso-v}/\delta L_{total}$ significantly smaller than that of control (untreated) RAPHCs ($p < 0.02$).

diminished the response to ionomycin; the calmodulin inhibitor, W-7 eliminated the iso-volumetric shortening (Farahbakhsh and Narins, 2006). In the present report, we demonstrated that RAPHCs have a rather low resting $[Ca^{2+}]_i$ of 66 ± 19 nM, which is comparable with the level reported for frogs vestibular hair cells (Ohtani et al., 1994), but somewhat lower than that observed in mammalian outer hair cells (Ashmore and Ohmori, 1990; Frolenkov et al., 2003). Ionomycin-induced shape change in RAPHCs, however, required micromolar $[Ca^{2+}]_i$ (see Results), suggesting possible involvement of medium-affinity mediators in this response. Here, we attempted to identify additional key steps in the calcium/calmodulin-dependent pathways that may contribute to the iso-volumetric shortening. Our results suggest both the myosin light chain kinase and a multifunctional Ca^{2+} /CaM-dependent kinase, as well as the myosin phosphatase participate in shaping the phase 1 response.

We tested the effects of three specific inhibitors of the two main classes of Ca^{2+} /CaM-dependent protein kinases, namely MLCK and multifunctional CaMKs. As yet there is no report demonstrating the presence of either MLCK or any CaMK in amphibian hair cells. However, immunological studies have suggested the presence of myosin light chain kinase in mammalian OHCs (Knipper et al., 1995), and have localized the Ca^{2+} /CaM-dependent protein kinase IV in the OHC cytoplasm (Koyama et al., 1999; Frolenkov et al., 2000). ML-7 is a specific MLCK inhibitor (Saitoh et al., 1987; Bain et al., 2003), whose effects on the slow motility in OHCs have been previously reported (Puschner and Schacht, 1997). This inhibitor, at 5 μ M concentration, while having no significant effect on the shape of RAPHCs when applied alone, abolished the iso-volumetric shortening in response to ionomycin (Figs. 4A and 6).

The two specific inhibitors for multifunctional CaMKs we used are KN-62 (Tokumitsu et al., 1990; Davies et al., 2000) and KN-93 (Sumi et al., 1991), of which the former is shown to inhibit the slow motility in OHCs (Puschner and Schacht, 1997; Minamino et al., 1998; Sziklai et al., 2001). The absence of a significant effect on RAPHCs by either of these two inhibitors, when applied alone, is not compatible with a role for a constitutively active CaMK in the

maintenance of RAPHCs' shape at the physiological levels of $[Ca^{2+}]_i$ and calmodulin.

The effects of these two CaMK inhibitors on the ionomycin-induced response were similar, and in none of the parameters we measured could a statistically significant difference between the two groups be shown. Both inhibitors eliminated phase 1 episode. Comparison of these inhibitors with ML-7 failed to establish a statistically significant difference with regard to any measured parameter. The combination of ML-7 and KN-62 produced an osmotic response to ionomycin which was in every respect similar to the effect of pretreatment with ML-7 alone (Figs. 4D and 6).

These results suggest, but clearly do not prove, that in RAPHCs, MLCK and CaM kinases constitute the primary pathways through which Ca^{2+} and calmodulin exert their effects on phase 1 response. Furthermore, they indicate that co-activation of both pathways is required for the expression of phase 1: inhibition of either pathway removed this phase (Fig. 4A–C); inhibiting both concurrently did not bring about a different outcome than blocking either pathway (Figs. 4D and 6). Thus, it appears that the transduction cascade mediating the phase 1 response utilizes a biochemical 'AND gate'. Since the most likely substrate for MLCK in the nonmuscle cells is the 20-KD myosin light chain (MLC, Means, 2000), we hypothesize that in RAPHCs, MLC constitutes the target of MLCK and CaMK activities involved in the iso-volumetric length change. It has been reported that in smooth muscle and nonmuscle cells, activation of multifunctional CaMKs can directly or indirectly lead to the phosphorylation of MLCK, MLC and myosin heavy chain (MHC). However, CaMK-dependent phosphorylation of MLCK has an inhibitory effect on the actin-dependent Mg^{2+} -ATPase activity of smooth muscle myosin II (for a review, see Pfitzer, 2001). Furthermore, in vertebrate nonmuscle cells, phosphorylation of MHC by CaMKs is reported to lead to either inhibition of (Sagara et al., 1983), or have no effect on (Tanaka et al., 1986) actin-dependent myosin Mg^{2+} -ATPase activity. These considerations lead to MLC as the primary candidate for CaMK-dependent activity mediating the phase 1 response (Fig. 7).

In smooth muscles, both MLCK and CaMK II phosphorylate MLC at a common site, resulting in enhancement of actin-activated Mg^{2+} -ATPase activity of myosin (Edelman et al., 1990). In pancreatic β cells, phosphorylation of MLC by MLCK requires low but suprabasal $[Ca^{2+}]_i$ ($<1 \mu M$), and saturates above $1 \mu M$, while phosphorylation by CaMK II requires $[Ca^{2+}]_i > 1 \mu M$, and saturates above $10 \mu M$ (Iida et al., 1997). This difference in sensitivity to the $[Ca^{2+}]_i$ can be explained by the observation that affinity of CaMKII for CaM is about 10 times lower than that of MLCK (Schulman and Hanson, 1993). However, it should be mentioned that when CaMKII is activated it undergoes autophosphorylation in a co-operative manner, and becomes autonomous (by increasing its affinity for calmodulin by almost three orders of magnitude), thus prolonging the response to a brief stimulatory spike in the $[Ca^{2+}]_i$ (Hanson et al., 1994). These characteristics of CaMKII has led us to hypothesize that in RAPHCs, the initial modest increase in the $[Ca^{2+}]_i$ induced by ionomycin, activates MLCK. However, phosphorylation of MLC by MLCK alone is not sufficient to produce an iso-volumetric shortening (Fig. 4B and C). Further increase in the $[Ca^{2+}]_i$ to micromolar levels is needed to activate a CaMK to supplement and prolong the phosphorylation of MLC, and therefore induce a sustained response. Conversely, in the absence of an MLCK-mediated phosphorylation of MLC (Fig. 4A), CaMK activity on its own is not capable of generating a discernable phase 1. According to this hypothesis, MLCK and CaMK form the 'AND gate' incorporated in

the Ca^{2+} /CaM-dependent pathway, and therefore their concerted activation is required for sufficient phosphorylation of MLC in RAPHCs (Fig. 7).

One possible reason for the inability of MLCK activity alone to generate a measurable response might be the presence of a constitutively active myosin light chain phosphatase (MLCP). The presence of MLCP in hair cells has not been reported. Therefore, in order to test whether MLCP is active in RAPHCs, we took advantage of the fact that the catalytic subunit of the MLCP is a type 1 protein phosphatase (PP1, Hartshorne et al., 2004). A hallmark of PP1 is its much higher susceptibility to inhibition by calyculin A, than by okadaic acid (Ishihara et al., 1989). In all five RAPHCs treated with calyculin A, and all five treated with okadaic acid, cells shortened during exposure to the inhibitor. However, the extent of shortening for calyculin A-treated cells was significantly larger than the length changes displayed during the previous period of exposure to the AP solution ($p < 0.015$), while that was not the case for cells treated with okadaic acid ($p > 0.35$). When these two groups were exposed to ionomycin, they both exhibited a phase 1 response. However, neither PP1 inhibitor significantly increased the extent of ionomycin-induced iso-volumetric shortening (Fig. 6), nor did they increase the rate of shortening (not shown).

The opposing effects of one of the PP1 inhibitors (calyculin A) and those of a CaMK inhibitor (KN-93; Fig. 5C), suggest a common substrate. Antagonistic effects of W-7 and okadaic acid have been observed by Frolenkov et al. (2000) using the cell membrane non-linear capacitance measurement in an OHC preparation. These investigators however concluded that the primary substrate for this phosphorylation/dephosphorylation process was the electromotile mechanism. In contrast, Borko et al. (2005) using a chemical and mechanical stimulation technique, found that okadaic acid blocked slow motility in OHCs. They concluded that calcium- and phosphorylation-dependent processes change the OHCs' lateral wall stiffness by modifying cytoskeletal proteins. Moreover, Minamino et al. (1998), investigating the osmotic shortening in OHCs induced by tetanic electrical field stimulation observed that calyculin A inhibited shortening apparently by decreasing the permeability to Cl^- . Since non-mammalian auditory hair cells appear to lack somatic electromotility (Köppl et al., 2004), our results cannot be explained by a shift in the operating point of the electromotile force. Furthermore, in our experiments on RAPHCs, neither calyculin A nor okadaic acid blocked phase 1 of slow motility. Finally, the iso-volumetric character of phase 1 shortening in RAPHCs argues against a major role for ionic channels. Therefore, we suggest that the common and immediate target of phosphorylation/dephosphorylation processes involved in phase 1 response is the myosin light chain (Fig. 7), even though it is quite plausible that the final effector of this pathway might be the hair cells' cytoskeletal lattice.

In summary, our results suggest that $[Ca^{2+}]_i$ increases in the frog's rostral amphibian papillar hair cells utilize a signal transduction pathway that includes myosin light chain kinase, multifunctional Ca^{2+} /CaM-dependent kinase(s) and myosin phosphatase to induce iso-volumetric length decreases. Furthermore, acetylcholine is known to induce a small shortening both in OHCs (Szonyi et al., 1999a; Frolenkov et al., 2000) and RAPHCs (Farahbakhsh and Narins, 2004). We have also observed that the effects of acetylcholine could be mimicked by two other cholinergic ligands, carbachol and DMPP. Whereas the effects of acetylcholine and carbachol were transient (even in the continued presence of agonists), DMPP-induced shortening was irreversible (Farahbakhsh and Narins, unpublished observations). Based on our present results, we surmise that small $[Ca^{2+}]_i$ increases produced by acetylcholine and its agonists are sufficient only for the activation of MLCK, but not CaMKs. Therefore, as suggested by the data in Fig. 5C, the utilization of the pathways discussed in this report by physiological stimuli requires inhibition of myosin phosphatase activity, an issue that

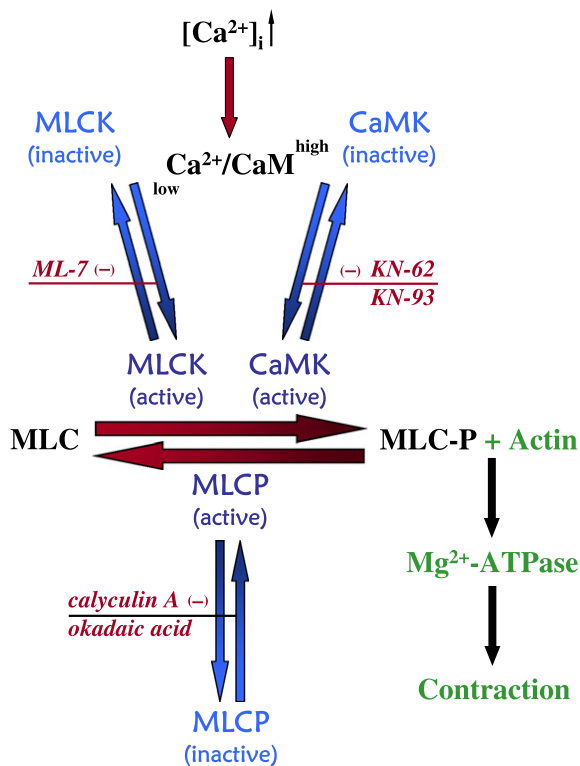


Fig. 7. A model for regulation of the Ca^{2+} /CaM-dependent iso-volumetric shortening in the frog rostral amphibian papillar hair cells. Low suprabasal concentration of Ca^{2+} /CaM activates myosin light chain kinase (MLCK). However, because of possible activity of the myosin light chain phosphatase (MLCP), phosphorylation of myosin light chain (MLC) by MLCK alone is not sufficient to trigger actin-activated myosin Mg^{2+} -ATPase. Full phosphorylation of MLC requires either higher concentrations of Ca^{2+} /CaM, and activation of a multifunctional Ca^{2+} /CaM-dependent kinase (CaMK) to overwhelm the phosphatase activity, or inhibition of the phosphatase activity in addition to modest $[Ca^{2+}]_i$ increase to trigger actomyosin-mediated contraction. The step-specific inhibitors (ML-7, KN-62, KN-93, calyculin A and okadaic acid) used in this work (printed in red and *italic* font), and the sites of their action (printed in blue and *Maiandra* font) are indicated. The right side of the model (in green, with textured arrows) is speculative at this point. (For interpretation of the references to colour in this figure legend, the reader is referred to the web version of this article.)

needs to be investigated. The general role of slow shape changes in hair cells and their contributions to the causal pathway leading to sound detection are currently under study.

Acknowledgement

This work was supported by National Institutes of Health Grant DC-00222.

Appendix A. Supplementary material

Supplementary data associated with this article can be found, in the online version, at doi:10.1016/j.heares.2008.04.007.

References

- Ashmore, J.F., Ohmori, H., 1990. Control of intracellular calcium by ATP in isolated outer hair cells of guinea-pig cochlea. *J. Physiol.* 428, 109–131.
- Bain, J., McLaughlan, H., Elliott, M., Cohen, P., 2003. The specificities of protein kinase inhibitors: an update. *Biochem. J.* 371, 199–204.
- Bernard, C., Ferrary, E., Sterkers, O., 1986. Production of endolymph in the semicircular canal of the frog *Rana esculenta*. *J. Physiol.* 371, 17–28.
- Blanchet, C., Erostequi, C., Sugasawa, M., Dulon, D., 1996. Acetylcholine-induced potassium current of guinea pig outer hair cells: its dependence on a calcium influx through nicotinic-like receptors. *J. Neurosci.* 16, 2574–2584.
- Borko, R., Batta, T.J., Sziklai, I., 2005. Slow motility, electromotility and lateral wall stiffness in the isolated outer hair cells. *Hear. Res.* 207, 68–75.
- Chertoff, M.E., Brownell, W.E., 1994. Characterization of cochlear outer hair cell turgor. *Am. J. Physiol.* 266, C467–C469.
- Dallos, P., Fakler, B., 2002. Prestin, a new type of motor protein. *Nat. Rev. Mol. Cell Biol.* 3, 104–111.
- Dallos, P., He, D.Z., Lin, X., Sziklai, I., Mehta, S., Evans, B.N., 1997. Acetylcholine, outer hair cell electromotility, and the cochlear amplifier. *J. Neurosci.* 17, 2212–2226.
- Davies, S.P., Reddy, H., Caivano, M., Cohen, P., 2000. Specificity and mechanism of action of some commonly used protein kinase inhibitors. *Biochem. J.* 351, 95–105.
- Deak, L., Zheng, J., Orem, A., Du, G.G., Aguinaga, S., Matsuda, K., Dallos, P., 2005. Effects of cyclic nucleotides on the function of prestin. *J. Physiol.* 563, 483–496.
- Dulon, D., Aran, J.M., Schacht, J., 1988. Potassium-depolarization induces motility in isolated outer hair cells by an osmotic mechanism. *Hear. Res.* 32, 123–129.
- Edelman, A.M., Lin, W.H., Osterhout, D.J., Bennett, M.K., Kennedy, M.B., Krebs, E.G., 1990. Phosphorylation of smooth muscle myosin by type II Ca²⁺/calmodulin-dependent protein kinase. *Mol. Cell. Biochem.* 97, 87–98.
- Erdahl, W.L., Chapman, C.J., Taylor, R.W., Pfeiffer, D.R., 1994. Ca²⁺ transport properties of ionophores A23187, ionomycin, and 4-BrA23187 in a well defined model system. *Biophys. J.* 66, 1678–1693.
- Farahbakhsh, N.A., Narins, P.M., 2004. Calcium-dependent contraction in hair cells of the amphibian papilla. *Assoc. Res. Otolaryngol. Abs.*, 1275.
- Farahbakhsh, N.A., Narins, P.M., 2006. Slow motility in hair cells of the frog amphibian papilla: Ca²⁺-dependent shape changes. *Hear. Res.* 212, 140–159.
- Farahbakhsh, N.A., Narins, P.M., 2007. Slow motility in hair cells of the frog amphibian papilla: myosin II-mediated shape change. *Assoc. Res. Otolaryngol. Abs.*, 473.
- Farahbakhsh, N.A., Simmons, D.D., Narins, P.M., 2006. Ca²⁺-dependent shortening and volume increase in auditory hair cells of the frog inner ear. *Assoc. Res. Otolaryngol. Abs.*, 1222.
- Flock, A., Flock, B., Ulfendahl, M., 1986. Mechanisms of movement in outer hair cells and a possible structural basis. *Arch. Otorhinolaryngol.* 243, 83–90.
- Frolenkov, G.I., Mammano, F., Belyantseva, I.A., Coling, D., Kachar, B., 2000. Two distinct Ca²⁺-dependent signaling pathways regulate the motor output of cochlear outer hair cells. *J. Neurosci.* 20, 5940–5948.
- Frolenkov, G.I., Mammano, F., Kachar, B., 2003. Regulation of outer hair cell cytoskeletal stiffness by intracellular Ca²⁺: underlying mechanism and implication for cochlear mechanics. *Cell Calcium* 33, 185–195.
- Gryniewicz, G., Poenie, M., Tsien, R.Y., 1985. A new generation of Ca²⁺ indicators with greatly improved fluorescence properties. *J. Biol. Chem.* 260, 3440–3450.
- Hanson, P.I., Meyer, T., Stryer, L., Schulman, H., 1994. Dual role of calmodulin in autophosphorylation of multifunctional CaM kinase may underlie decoding of calcium signals. *Neuron* 12, 943–956.
- Hartshorne, D.J., Ito, M., Erdodi, F., 2004. Role of protein phosphatase type 1 in contractile functions: myosin phosphatase. *J. Biol. Chem.* 279, 37211–37214.
- He, D.Z., Dallos, P., 1999. Somatic stiffness of cochlear outer hair cells is voltage-dependent. *Proc. Natl. Acad. Sci. USA* 96, 8223–8228.
- He, D.Z., Jia, S., Dallos, P., 2003a. Prestin and the dynamic stiffness of cochlear outer hair cells. *J. Neurosci.* 23, 9089–9096.
- He, D.Z., Beisel, K.W., Chen, L., Ding, D.L., Jia, S., Fritzsche, B., Salvi, R., 2003b. Chick hair cells do not exhibit voltage-dependent somatic motility. *J. Physiol.* 546, 511–520.
- Housley, G.D., Greenwood, D., Ashmore, J.F., 1992. Localization of cholinergic and purinergic receptors on outer hair cells isolated from the guinea-pig cochlea. *Proc. R. Soc. Lond. B Biol. Sci.* 249, 265–273.
- Iida, Y., Senda, T., Matsukawa, Y., Onoda, K., Miyazaki, J.I., Sakaguchi, H., Nimura, Y., Hidaka, H., Niki, I., 1997. Myosin light-chain phosphorylation controls insulin secretion at a proximal step in the secretory cascade. *Am. J. Physiol.* 273, E782–E789.
- Ishihara, H., Martin, B.L., Brautigam, D.L., Karaki, H., Ozaki, H., Kato, Y., Fusetani, N., Watabe, S., Hashimoto, K., Uemura, D., et al., 1989. Calyculin A and okadaic acid: inhibitors of protein phosphatase activity. *Biochem. Biophys. Res. Commun.* 159, 871–877.
- Iwasa, K.H., Chadwick, R.S., 1992. Elasticity and active force generation of cochlear outer hair cells. *J. Acoust. Soc. Am.* 92, 3169–3173.
- Kalinec, F., Zhang, M., Urrutia, R., Kalinec, G., 2000. Rho GTPases mediate the regulation of cochlear outer hair cell motility by acetylcholine. *J. Biol. Chem.* 275, 28000–28005.
- Knipper, M., Zimmermann, U., Kopschall, I., Rohbock, K., Jungling, S., Zenner, H.P., 1995. Immunological identification of candidate proteins involved in regulating active shape changes of outer hair cells. *Hear. Res.* 86, 100–110.
- Köppl, C., Forge, A., Manley, G.A., 2004. Low density of membrane particles in auditory hair cells of lizards and birds suggests an absence of somatic motility. *J. Comp. Neurol.* 479, 149–155.
- Koyama, M., Spicer, S.S., Schulte, B.A., 1999. Immunohistochemical localization of Ca²⁺/calmodulin-dependent protein kinase IV in outer hair cells. *J. Histochem. Cytochem.* 47, 7–12.
- Lim, D.J., Kalinec, F., 1998. Cell and molecular basis of hearing. *Kidney Int. Suppl.* 65, S104–S113.
- Means, A.R., 2000. Regulatory cascades involving calmodulin-dependent protein kinases. *Mol. Endocrinol.* 14, 4–13.
- Minamino, M., Hara, M., Ohnishi, S., Irie, T., Yamashita, T., Minato, A., Inagaki, C., 1998. Effects of protein kinase and phosphatase inhibitors on slow shortening of guinea pig cochlear outer hair cells. *Brain Res.* 781, 275–283.
- Miralem, T., Templeton, D.M., 1998. Heparin inhibits Ca²⁺/calmodulin-dependent kinase II activation and c-fos induction in mesangial cells. *Biochem. J.* 330, 651–657.
- Ohtani, M., Devau, G., Lehouelleur, J., Sans, A., 1994. Cholinergic agonists increase intracellular calcium concentration frog vestibular hair cells. *Hear. Res.* 80, 167–173.
- Pfitzer, G., 2001. Invited review: regulation of myosin phosphorylation in smooth muscle. *J. Appl. Physiol.* 91, 497–503.
- Puschner, B., Schacht, J., 1997. Calmodulin-dependent protein kinases mediate calcium-induced slow motility of mammalian outer hair cells. *Hear. Res.* 110, 251–258.
- Reiter, E.R., Liberman, M.C., 1995. Efferent-mediated protection from acoustic overexposure: relation to slow effects of olivocochlear stimulation. *J. Neurophysiol.* 73, 506–514.
- Sagara, J., Nagata, K., Ichikawa, Y., 1983. Phosphorylation of the myosin heavy chain. Its effect on actin-activated Mg²⁺-stimulated ATPase in leukaemic myeloblasts. *Biochem. J.* 214, 839–843.
- Saitoh, M., Ishikawa, T., Matsushima, S., Naka, M., Hidaka, H., 1987. Selective inhibition of catalytic activity of smooth muscle myosin light chain kinase. *J. Biol. Chem.* 262, 7796–7801.
- Schacht, J., Fessenden, J.D., Zajic, G., 1995. Slow motility of outer hair cells. In: Flock, A., Ottoson, D., Ulfendahl, M. (Eds.), *Active Hearing*, vol. 65. Pergamon, Oxford, pp. 209–220.
- Schulman, H., Hanson, P.I., 1993. Multifunctional Ca²⁺/calmodulin-dependent protein kinase. *Neurochem. Res.* 18, 65–77.
- Simmons, D.D., Bertolotto, C., Leong, M., 1995. Synaptic ultrastructure within the amphibian papilla of *Rana pipiens pipiens*: Rostrocaudal differences. *Aud. Neurosci.* 1, 183–193.
- Sumi, M., Kiuchi, K., Ishikawa, T., Ishii, A., Hagiwara, M., Nagatsu, T., Hidaka, H., 1991. The newly synthesized selective Ca²⁺/calmodulin dependent protein kinase II inhibitor KN-93 reduces dopamine contents in PC12h cells. *Biochem. Biophys. Res. Commun.* 181, 968–975.
- Sziklai, I., Szonyi, M., Dallos, P., 2001. Phosphorylation mediates the influence of acetylcholine upon outer hair cell electromotility. *Acta Otolaryngol.* 121, 153–156.
- Szonyi, M., Csermely, P., Sziklai, I., 1999a. Acetylcholine-induced phosphorylation in isolated outer hair cells. *Acta Otolaryngol.* 119, 185–188.
- Szonyi, M., He, D.Z., Ribari, O., Sziklai, I., Dallos, P., 1999b. Cyclic GMP and outer hair cell electromotility. *Hear. Res.* 137, 29–42.
- Szonyi, M., He, D.Z., Ribari, O., Sziklai, I., Dallos, P., 2001. Intracellular calcium and outer hair cell electromotility. *Brain Res.* 922, 65–70.
- Tanaka, E., Fukunaga, K., Yamamoto, H., Iwasa, T., Miyamoto, E., 1986. Regulation of the actin-activated Mg-ATPase of brain myosin via phosphorylation by the brain Ca²⁺, calmodulin-dependent protein kinases. *J. Neurochem.* 47, 254–262.
- Tokumitsu, H., Chijiwa, T., Hagiwara, M., Mizutani, A., Terasawa, M., Hidaka, H., 1990. KN-62, 1-[N,O-bis(5-isoquinolinesulfonyl)-N-methyl-L-tyrosyl]-4-phenylpiperazine, a specific inhibitor of Ca²⁺/calmodulin-dependent protein kinase II. *J. Biol. Chem.* 265, 4315–4320.
- Tsien, R.Y., Rink, T.J., Poenie, M., 1985. Measurement of cytosolic free Ca²⁺ in individual small cells using fluorescence microscopy with dual excitation wavelengths. *Cell Calcium* 6, 145–157.
- Zhang, M., Kalinec, G.M., Urrutia, R., Billadeau, D.D., Kalinec, F., 2003. ROCK-dependent and ROCK-independent control of cochlear outer hair cell electromotility. *J. Biol. Chem.* 278, 35644–35650.